Desalination and Water Treatment
www.deswater.com

doi:10.5004/dwt.2016.11035

61 (2017) 284–292
January

Prediction of cathodic Cu^{2+} reduction in a laboratory filter-press electrolyser by computational fluid dynamics modelling

H.I. Navarro[a], S. Silva-Martínez[b], J.A. Hernández[b], F.Z. Sierra[b], A. Alvarez-Gallegos[b,*]

[a]*Posgrado en Ingeniería y Ciencias Aplicadas FCQeI-CIICAp*
[b]*Centro de Investigación en Ingeniería y Ciencias Aplicadas*
Universidad Autónoma del Estado de Morelos, Av. Universidad 1001, Cuernavaca Morelos, 62209. Mexico
Tel. +52 777 329 7084; Fax +52 777 329 7984; email: aalvarez@uaem.mx

Received 11 April 2015; accepted 1 May 2016

ABSTRACT

Cathodic electrodeposition of metal ions can be achieved in parallel plate reactors. The reactor duty is enhanced when it is operated under limiting current conditions at the cathode. Such conditions are closely related to the fluid pattern over the entire cathode area. In this work, the theoretical feasibility for the removal of Cu^{2+} ions in an electrochemical reactor at laboratory level was analyzed as a function of the flow pattern. A commercial computational fluid dynamics code (ANSYS Fluent) was used to describe the hydrodynamic as the electrolyte passes through a laboratory electrochemical reactor (channel reactor: 0.10 m length, 0.05 m width, 0.01 m depth and electrode area 0.005 m^2). The simulation was performed at mean linear inlet flow velocities between 0.011 and 0.056 m s^{-1}. The flow predictions show how the development of the flow pattern is affected by both the manifold and the flow velocity. It was possible to estimate that the fluid flow was developed over the 90, 80 and 70% of the cathode area when the mean linear inlet flow were 0.011, 0.033 and 0.056 m s^{-1}, respectively. Under these hydrodynamic conditions, the electrochemical reactor performance will be maximized because it was expected to have a uniform limiting current density over the cathode area according to the estimated percentages mentioned before. In the same range of linear flow velocities, a uniform limiting current for cathodic Cu^{2+} reduction was experimentally obtained, as expected.

Keywords: Copper removal; Computational fluid dynamics; Cell design; Mass transport; Flow patterns

1. Introduction

Most of the heavy-metal ions (i.e. Cu, Ag, Pb) in industrial effluent are harmful when they are discharged to the environment [1]. Among the available technological methods for metal removal from diluted solutions the electrochemical technology is well positioned [2–4]. The main advantages of this approach include metal recovery in pure form, low operating costs and no sludge disposal problems. One of the earliest studies on this subject was documented more than 50 years ago [5]. Since then, a huge amount of work focused on stripping of metals from water streams has been performed. Early studies were focused on Cu [6], Ag and Pb [6,7] deposition. Recently, several electrodeposition techniques have been applied to remove heavy metals from aqueous solutions, among them it can be mentioned Zn [8,9], Co [8,10] and Cu [11].

The cathodic reduction of heavy metal cations is one of the most important electrochemical procedures. The goal of this process is to control the mass transport to the cathode surface [12,13] by means of the limiting current (I_L) concept. For a given concentration of the electroactive species the I_L is linked to both, the electrode area (A_e) and the mass transfer coefficient (k_m). These two parameters are linked to the

*Corresponding author.

Presented at EuroMed 2015: Desalination for Clean Water and Energy Palermo, Italy, 10–14 May 2015. Organized by the European Desalination Society.

reactor design and the flow pattern. A correct reactor design requires ensuring a fully developed flow condition over the most part of the cathode surface. Therefore, the optimum performance of a cathodic reduction is achieved when main parameters, that are a function of fluid dynamics (I_L and k_m), will be uniform along the electrode surface. As a result, the mass transfer, from the bulk solution to the electrode surface is going to be uniform.

The objective of this paper is to evaluate the maximum cathode area at which the flow pattern describes a fully developed laminar flow (describing a parabolic profile). The flow pattern will be evaluated by means of a computational fluid dynamics (CFD) tool as a function of the electrolyte Reynolds number (representing the ratio of inertial force to friction force) expressed by *Re*. In this way, a selected *Re* range will define the theoretical conditions at which the electrochemical reactor should work with a uniform I_L, assuring a good k_m and therefore a suitable cathodic Cu^{2+} reduction. Theoretical values will be compared against experimental ones.

2. Theoretical approach

2.1. Mass transfer coefficient and hydrodynamics

For a fully developed laminar flow, the limiting current (I_L) and the mass transfer coefficient (k_m) are related by the following equation [13,14]:

$$I_L = n\mathrm{F}Aek_m\mathrm{C}_{Cu^{2+}} \tag{1}$$

where *n* is the number of electrons, F is the Faraday constant, *Ae* is the electrode surface and $C_{Cu^{2+}}$ is the cation copper concentration in the bulk solution. The characteristic mean linear flow velocity ($\overline{v}$) of the electrolyte (obtained as a relation of the volumetric flow rate divided by the cross-sectional area of the reactor channel) is linked to the k_m by means of the following equation [15]:

$$k_m = a\left(\overline{v}\right)^b \tag{2}$$

where *a* and *b* are experimental constants that take into account the electrolyte transport properties (*Sc* number) and the geometry of the electrochemical reactor (the equivalent hydraulic diameter, d_e).Under these conditions k_m and the experimental constants can be evaluated in an electrochemical reactor from correlations involving dimensionless parameters [15].

$$Sh = \mathrm{a}\,Re^{\mathrm{b}}Sc^{\mathrm{c}}Le^{\mathrm{e}} \tag{3}$$

where a, b, c, e are as well experimental constants, *Sh* is the Sherwood number (the ratio of the mass transfer rate to the diffusion rate), *Le* is the ratio of hydraulic diameter to the length of the electrode in the direction of the flow and the rest of the parameters were already defined. If the parameter *Re* is measured from $\overline{v}$, the resulting numerical value will be named nominal *Re*. In the same way, if the parameter *Sh* is evaluated from a nominal *Re*, the resulting numerical value will be named averaged *Sh*. Equations (2) and (3) describe the mass transport in fully developed laminar flow. However, the sudden expansion of fluid flow is the more convenient method to introduce the electrolyte to an electrochemical reactor. As a result, the flow pattern at the cell entrance is characterized by the presence of a recirculation of the fluid. Thus, the *Re* becomes a function of the expansion geometry and several attempts have been made to evaluate this phenomenon. The main problem is the assessment of the minimum distance from the reactor entrance, from which, a fully developed flow starts.

2.2. Fully developed laminar flow

The flow pattern inside of an electrochemical reactor becomes unstable above a critical *Re* (Re_{Crit}). This parameter is not a constant; it is a function of the geometry of the manifold used to introduce/remove the electrolyte from an electrochemical reactor. At low Reynolds numbers ($Re < Re_{Crit}$) flows are laminar and at higher Reynolds numbers ($Re > Re_{Crit}$) flows are turbulent. In the laminar regime the flow is smooth and adjacent layers of fluid slide past each other in an orderly fashion. Moreover, if the applied boundary conditions do not change with time/distance, the flow develops completely with a parabolic profile. Therefore, the precise Re_{Crit} assessment is very important to define the flow regime inside the electrochemical reactor. Several procedures have been employed to evaluate the minimum downstream length required for a fully developed laminar flow. Among them it can be mentioned the following criterion [16]:

$$L^* = 0.06\left(Re\right)d \tag{4}$$

where L^* is the minimum entrance length, *d* is the diameter of a circular pipe. The assessment of the minimum entrance length depends only on *Re* and *d*. Therefore, the flow behavior differences between electrode surface and bulk solution, as well as near the manifolds are ignored. These limitations were recognized by Pickett and Wilson [16]. In theory flow dispersion models are able to describe a fully developed laminar flow [17]. However the inherent difficulties of this flow model for the correct interpretations of the experimental data [18] make them unpractical.

As it was stressed before, the *Re* is a function of the fluid recirculation at the reactor entrance. In order to evaluate the expansion factor of the flow, certain correlation between the manifold geometries and some measurable quantities, such as heat [19] or mass transports coefficients [20,21] were developed for different entry arrangements, see the following equation:

$$ShSc^{-1/3} = 0.11Re^{0.73}\left(\frac{d_e}{D_e}\right)^{-1} \tag{5}$$

where (d_e/D_e) is the ratio of entrance equivalent diameter to the electrochemical cell equivalent diameter. When the cell entry is limited to one circular hole, Eq. (5) is able to describe the flow pattern, but it fails for a slit-type cell entrance. When a new expansion factor was included in Eq. (5) the theoretical evolution of flow pattern was well described for

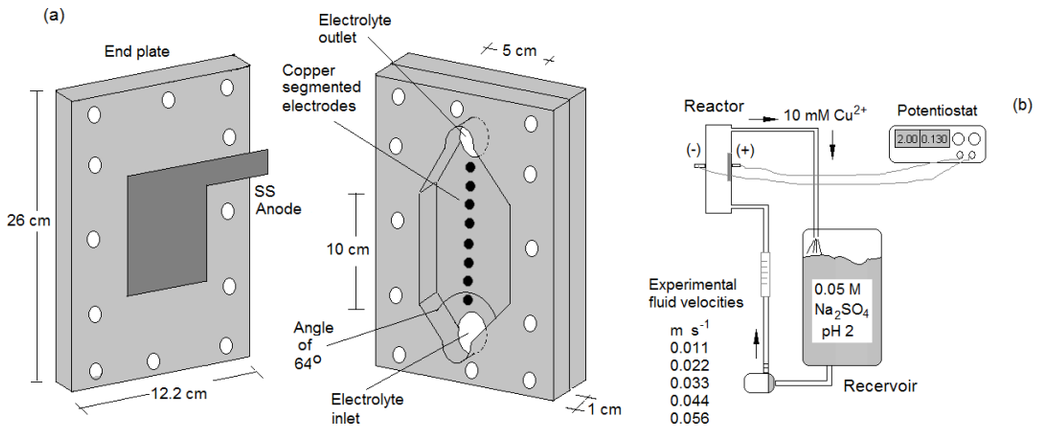

Fig. 1. Main features of the electrochemical reactor and its circuit hydraulic.

tube-type entrance and slit-type entrance [22]. However, the improved equation fails to describe the flow pattern in more complicated reactor entrances. Therefore, an improved geometrical manifold parameter was proposed and included in a new equation. When this approach was applied to an electrochemical reactor the diagnosis obtained described a jet stream and vortex at the cell entrance [23]. Although this information may be useful for an experienced designer, for others it is very subjective. Indeed, a theoretical reactor design must include the minimum required length of the calming zone to subdue disturbances. This task can be solved by means of CFD.

2.3. Computational fluid dynamics

CFD offers the possibility for reactor designing objectives [24] and to evaluate under realistic conditions, the flow pattern and its effect on mass transport in developing fluids along a reactor [25–27]. In this study ANSYS Fluent (v6.3.26) was used to provide a numerical description of the flow patterns in a laboratory reactor. The most important characteristics of the reactor are summarised in Fig. 1a: the electrolyte inlet/outlet has an angle of 64° and in between the channel reactor (0.1 m length x 0.05 m width x 0.01 m depth). The electrolyte is distributed to the reactor channel by the inlet as shown in Fig. 1a. When the electrolyte is pumped through the channel from the bottom to the top a flow pattern develops along the channel length and width as a function of the flow rate.

3. Modelling conditions

The fluid flow can be modelled from the basic principles of conservation of mass, momentum and energy [28] and applying the same methodology described elsewhere [25–27]. However, the most important modelling activities are the reactor geometry definition and grid generation. This includes the subdivision geometry into non-overlapping 548,202 hexagonal cells; definition of the electrolyte properties (described in Table 1); selection of appropriated boundary conditions (derived from data in Table 1) such as the electrolyte mass flux (kg s^{-1}) at the reactor inlet.

In order to describe a realistic flow pattern in the reactor, the following set of five partial differential equations is needed: mass conservation, x, y and z momentum equations and the energy balance equation. However, some simplifications can be made if the following assumptions are taken: i) steady state is assumed in the fluid flow equations while the time variable is not considered, ii) the temperature, density and viscosity of the fluid are constant, iii) natural convection is neglected due to the predominance of

Table 1
Main experimental conditions

Parameter	Physical properties of the electrolyte				
	ρ kg m^{-3}	μ kg m^{-1} s^{-1}	*Sc* ($\mu/\rho D_{Cu^{2+}}$)	$D_{Cu^{2+}}$ (m^2 s^{-1})	*Re* ($v\rho d_e/\mu$)
Value	1099	1.1 x 10^{-3}	1494	6.4 x 10^{-10}	170–1000
Characteristic mean linear flow velocities ($\overline{v}$) of the electrolyte, volumetric flow rate (Q) and nominal *Re* number in the laboratory reactor					
Q (m^3 s^{-1})	5.56 x 10^{-6}	1.11 x 10^{-5}	1.67 x 10^{-5}	2.22 x 10^{-5}	2.78 x 10^{-5}
$\overline{v}$ (m s^{-1})	0.011	0.022	0.033	0.044	0.056
Nominal *Re*	194	387	581	775	969

forced convection and iv) there is no linkage between the energy equation, the mass conservation and the momentum equations. The energy equation needs to be solved alongside the others if the problem involves heat transfer. Therefore, the system is reduced to four partial differential equations. In a laminar regime, Newtonian incompressible fluid flow behaviour is completely described by the Navier-Stokes equations:

$$\frac{\partial v_i}{\partial x_i} = 0 \tag{6}$$

$$\frac{\partial}{\partial x_i}\left(v_i v_j\right) = -\frac{\partial}{\partial x_j} p\delta_{ij} + \frac{\partial}{\partial x_j} \tau\delta_{ij} \tag{7}$$

where v_i, x_i are the velocity vector and its position (i = x, y, z) respectively, p is the pressure and τ is a viscous stress term.

As mentioned previously, all flows encountered in engineering practice become unstable above the Re_{Crit}. Therefore, the flow pattern described by the electrolyte when it is pumped through the variable reactor geometry is turbulent, even if the Reynolds number is well below 2000. Therefore, extra tools are needed to describe the effects of turbulence. However, commercial CFD packages offer the possibility of using several turbulence models that can be solved in three dimensions alongside the N avier-Stokes equations. Among the models it can be mentioned the RNG model. It was used to solve terms that appear when the set of Navier-Stokes equations are applied to flow regions which are dominated by strong velocity gradients, like vortex flows that characterize recirculation flow regions or boundary layer separation flows [25,27]. In this work, the renormalization-group (RNG) model was coupled to Navier-Stokes equations for modelling the fluid flow through the reactor shown in Fig. 1.

4. Experimental details

4.1. Solutions

They were prepared using distilled water and the following reagents: Na_2SO_4, $CuSO_4$, H_2SO_4 all of them supplied by Aldrich.

4.2. Electrodes and reactor

The anode was made of a sheet (0.10 m x 0.05 m) of stainless steel. Ten circular cathodes (0.01 m diameter) made of copper were imbibed into the center of the channel width but at different position along the channel length, as shown in Fig. 1a. The dimensions of the plate, in which the reactor channel was built, are: 0.26 m length, 0.122 m width and 0.10 m depth. The rest of the geometrical details were already mentioned. The calomel was used as a reference electrode. The working electrolyte (0.05M Na_2SO_4, 10mM $CuSO_4$, pH 2) was recirculated through the reactor by means of an Iwaki magnet pump MD-10L. A sketch of the hydraulic circuit is shown in Fig. 1b. All electrochemical experiments were controlled by a potentiostat (AMEI model 553).

4.3. Procedures

Experimental mass transport studies were performed by the limiting current technique [13]. The working electrolyte was deoxygenized before the mass transport measurements. The cathode energies were swept from 0 to –1.0 V (vs calomel) and the limiting current was determined for the cathodic reduction of Cu^{2+} on circular copper electrodes. This procedure was repeated for all the volumetric flow rates described in Table 1.

5. Results and discussion

5.1. Simulation of the flow pattern

The objective of CFD is to evaluate: a) the entry region where the flow develops; b) the region where the fluid flow is developed; c) the region where the outlet port remove electrolyte from the reactor and affect the fluid flow pattern. At all volumetric flow rates, local flow velocities can be obtained as a function of the channel length (0.10 m), width (0.050 m) and depth (0.010m). Then, they can be represented in 2D/3D graphics showing contours of x-velocity, velocity vectors and velocity profile for a given channel depth along the channel width. The fluid flow was assessed in different points located in some selected planes along the channel length.

The length of the electrolyte compartment, from the inlet port to the outlet port, is divided in 10 perpendicular planes to the direction of the fluid flow, see two of them (P3 and P4) in a partial channel representation in Fig. 2. The first two of them (P1 and P2) are located at 2 and 0.5 cm respectively, before the channel entry; they are not represented in Fig. 2.

In fact, P1 is located at the centre of the electrolyte compartment, where the inlet port is placed. In this position, at all volumetric flow rates, a turbulent regime is always expected because the flow direction changes abruptly. From this point, the electrolyte is distributed, toward the reactor channel, through a 64° divergent duct. Following this direction, the fluid flow reaches the plane P2. At this point, the flow pattern should be still turbulent. The following planes, P3 to P8, are located in the reactor channel at the following distances 1, 3, 5, 7, 9 and 10 cm, respectively. In this channel zone (10 cm long), the flow pattern should form a fully developed flow, for some of the volumetric flow rates of Table 1. Beyond 10 cm (P8), the electrolyte is distributed, toward the outlet port through a 64° convergent duct. From P9 to P10, the flow pattern should be turbulent again. For a given perpendicular plane (i.e. P3 in Fig. 2), local velocities are numerically evaluated in 18 positions (P1 to P18) along the channel depth obtaining a velocity profile (VP) in the z direction. This procedure is systematic repeated at different positions along the channel width and 11 VP are obtained for P3. Applying the same procedure, 11 VP are obtained for P4 and so on for all 10 perpendicular planes to the direction of the fluid flow. Therefore, a flow pattern is obtained for a given flow rate. In the following section, a set of ($\overline{v}$) will be discussed. Some important VPs corresponding to the most representative set of perpendicular planes located at the key electrolyte compartment distances are discussed. From Fig. 2 it can be seen the angle for graphical representation in 2D (channel depth vs local velocity) for a given set of 11 VPs along the channel width.

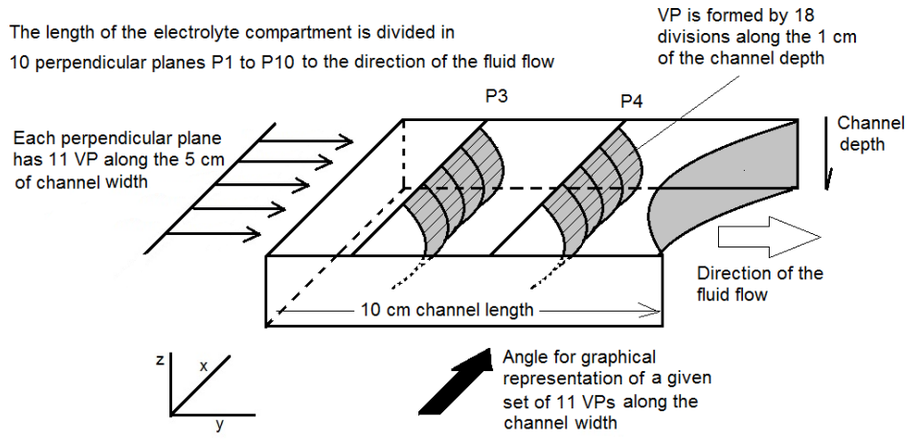

Fig. 2. A partial reactor channel representation and the locations of key points.

0.011 m s^{-1}. The set of VPs formed at 2 and 0.5 cm before the channel entry and at the first 1 cm in the channel length are represented in Figs. 3a–c, respectively.

As expected, the first two set of VPs describe a turbulent flow, however, the third set of VPs describe a parabolic profile, characteristic of a developed fluid flow. It can be seen that the lowest velocities are found near the four channel walls, at 0.25 m, 4.75 cm, for the channel width and 1.0 cm, 0.0 cm for the channel depth. The same flow pattern is found for the rest of the channel. Fig. 3d shows that at the end of the channel length (10 cm), the parabolic profile is not affected by the outlet effect. For this $\overline{v}$ examined it can be concluded that 9 cm, of the 10 cm channel length, present a developed fluid flow. Giving 45 cm^2 of cathode area at which the flow pattern describes a fully developed laminar flow, that is 90% of the channel surface.

0.022–0.056 m s^{-1}. Applying the same method for the whole range of $\overline{v}$ it can be seen that before the channel entry all VPs describe a turbulent flow. Additionally, the minimum downstream length required for a fully developed laminar flow is smoothly increasing as a function of the flow rate. As a consequence, the area at which the flow pattern describes a fully developed laminar flow decreases. The most important findings are summarized for a representative set of flows. For a $\overline{v}$ = 0.033 ms^{-1}, Fig. 4a shows aset of VPs describing a quasi-parabolic profile at 2 cm in the channel length. However, from a few fractions of a centimetre ahead to the end of the channel, the set of VPs describe a parabolic profile and they are not affected by the outlet effect. Fig. 4b shows a set of VPs describing a parabolic profile at the end of the channel. Under these conditions, the flow pattern describes a fully developed laminar flow above 40 cm^2 of the channel area, representing the 80% of the total channel area available.

For a $\overline{v}$ = 0.056 ms^{-1}, Fig. 5a shows a set of VPs describing a quasi-parabolic profile at 3 cm in the channel length.

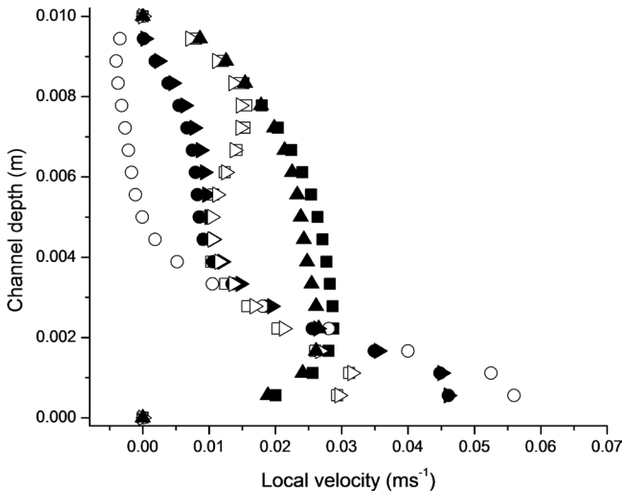

Fig. 3a. Seven VPs along channel depth at 2 cm before the cannel entry and the following channel width: ● 0.01 m, ○ 0.015 m, ▶ 0.02 m, ▷ 0.025 m, ▲ 0.03 m, △ 0.035 m, ★ 0.04 m. $\overline{v}$ = 0.011 ms^{-1}.

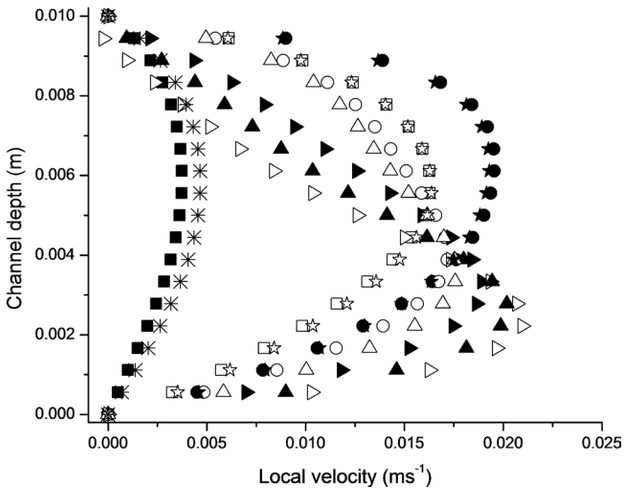

Fig. 3b. Eleven VPs along channel depth at 0.5 cm before the channel entry and the following channel width: ■ 0.0025 m, □ 0.005 m, ● 0.01 m, ○ 0.015 m, ▶ 0.02 m, ▷ 0.025 m, ▲ 0.03 m, △ 0.035 m, ★ 0.04 m, ☆ 0.045 m, ✱ 0.0475 m. $\overline{v}$ = 0.011 ms^{-1}.

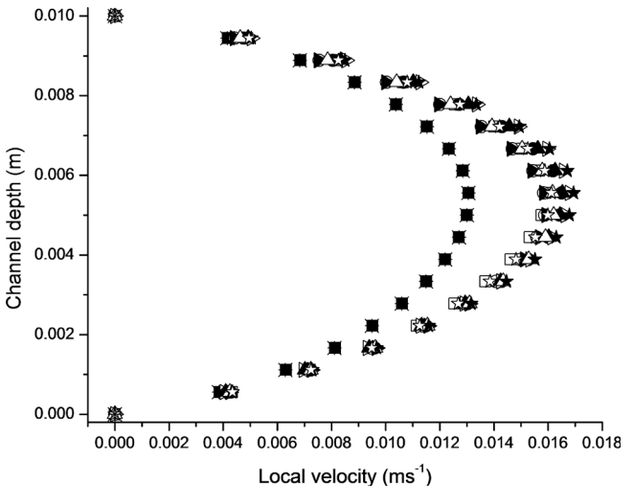

Fig. 3c. Eleven VPs along channel depth at 1.0 cm of the channel entry and the following channel width: ■ 0.0025 m, □ 0.005 m, ● 0.01 m, ○ 0.015 m, ▶ 0.02 m, ▷ 0.025 m, ▲ 0.03 m, △ 0.035 m, ★ 0.04 m, ☆ 0.045 m, ✱ 0.0475 m. $\overline{v}$ = 0.011 ms^{-1}.

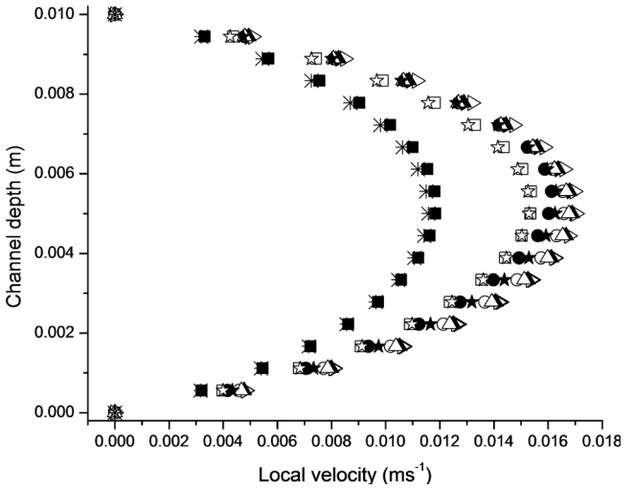

Fig. 3d. Eleven VPs along channel depth at 10 cm of the channel entry and the following channel width: ■ 0.0025 m, □ 0.005 m, ● 0.01 m, ○ 0.015 m, ▶ 0.02 m, ▷ 0.025 m, ▲ 0.03 m, △ 0.035 m, ★ 0.04 m, ☆ 0.045 m, ✱ 0.0475 m. $\overline{v}$ = 0.011 ms^{-1}.

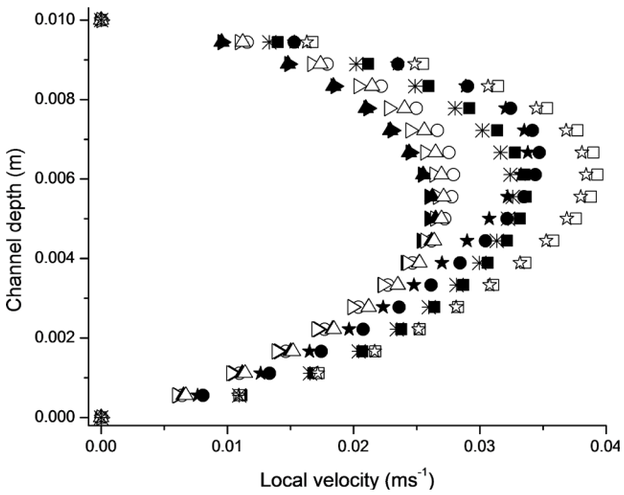

Fig. 4a. Eleven VPs along channel depth at 2.0 cm of the channel entry and the following channel width: ■ 0.0025 m, □ 0.005 m, ● 0.01 m, ○ 0.015 m, ▶ 0.02 m, ▷ 0.025 m, ▲ 0.03 m, △ 0.035 m, ★ 0.04 m, ☆ 0.045 m, ✱ 0.0475 m. $\overline{v}$ = 0.033 ms^{-1}.

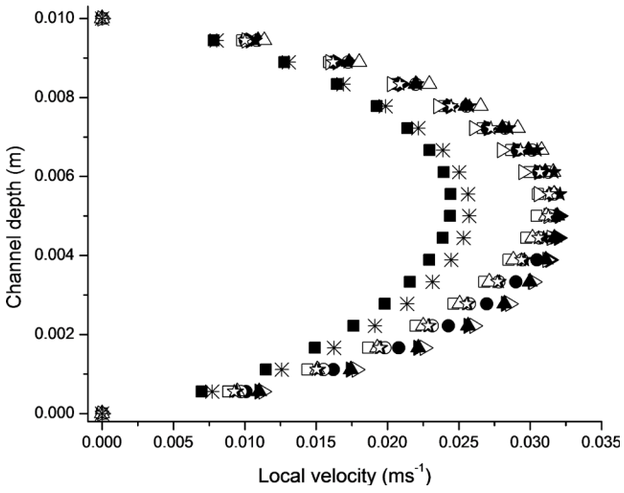

Fig. 4b. Eleven VPs along channel depth at 10.0 cm of the channel entry and the following channel width: ■ 0.0025 m, □ 0.005 m, ● 0.01 m, ○ 0.015 m, ▶ 0.02 m, ▷ 0.025 m, ▲ 0.03 m, △ 0.035 m, ★ 0.04 m, ☆ 0.045 m, ✱ 0.0475 m. $\overline{v}$ = 0.033 ms^{-1}.

From this channel position to the end of the channel, the set of VPsdescribe a parabolic profile and they are not affected by the outlet effect. Fig. 5b shows a set of VPs describing a parabolic profile at the end of the channel. Under these conditions the available area, under a fully developed laminar flow, is 35 cm^2 (70%).

The main conclusions so far are the following: The electrolyte inlet effect on the minimum distance of the reactor channel, from which a fully developed flow starts, is a function of the nominal *Re*. For the following set of nominal *Re* the following minimum distances of channel length were found: 1 cm for 194 < *Re* < 387, 2 cm for 387 < *Re* < 775 and 3 cm for 775 < *Re* < 969. Therefore, in the three nominal *Re* regions mentioned the electrochemical reactor should work with a uniform I_L, assuring a good k_m and therefore a suitable cathodic Cu^{2+} reduction. However, at low nominal *Re* regime, the available cathode area will be higher.

5.2. Experimental mass transport studies

The cathodic Cu^{2+} reduction on a set of circular copper electrodes were performed. The electrodes were located at the center of the channel width but at different position along the channel length. Their limiting current were recorded as a function of the nominal *Re*. The first circular electrode (P1) was fixed in the electrolyte compartment, where the inlet port is placed (2 cm before the channel entry). According to CFD analysis (Fig. 3a) on P1, a turbulent regime was always

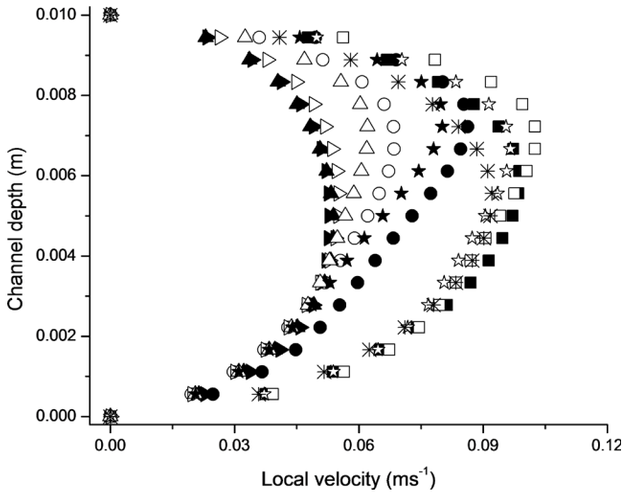

Fig. 5a. Eleven VPs along channel depth at 3.0 cm of the channel entry and the following channel width: ■ 0.0025 m, □ 0.005 m, ● 0.01 m, ○ 0.015 m, ▶ 0.02 m, ▷ 0.025 m, ▲ 0.03 m, △ 0.035 m, ★ 0.04 m, ☆ 0.045 m, ✱ 0.0475 m. $\overline{v}$ = 0.056 ms^{-1}.

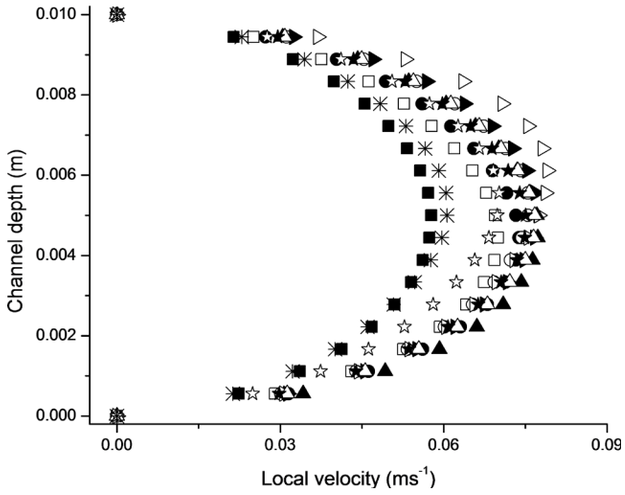

Fig. 5b. Eleven VPs along channel depth at 10.0 cm of the channel entry and the following channel width: ■ 0.0025 m, □ 0.005 m, ● 0.01 m, ○ 0.015 m, ▶ 0.02 m, ▷ 0.025 m, ▲ 0.03 m, △ 0.035 m, ★ 0.04 m, ☆ 0.045 m, ✱ 0.0475 m. $\overline{v}$ = 0.056 ms^{-1}.

found, at all volumetric flow rates. Fig. 6a shows that for nominal *Re* > 581 (curves marked with ▲, ■, ∗) the limiting currents for Cu^{2+}cathodic reduction are rather undefined in P1. However, for nominal *Re* < 581 the limiting currents are better defined.

Fig. 6b shows that for all nominal *Re* examined (except for nominal *Re* = 969) the limiting currents for Cu^{2+}cathodic reduction on electrode P2 (0.5 cm before the channel entry) are well defined. Experimental results suggest that the mass transport is carried out in a fully developed laminar flow (Eqns. 2 and 3). According to CFD analysis (Fig. 3b) on P2 the fluid flow is not developed.

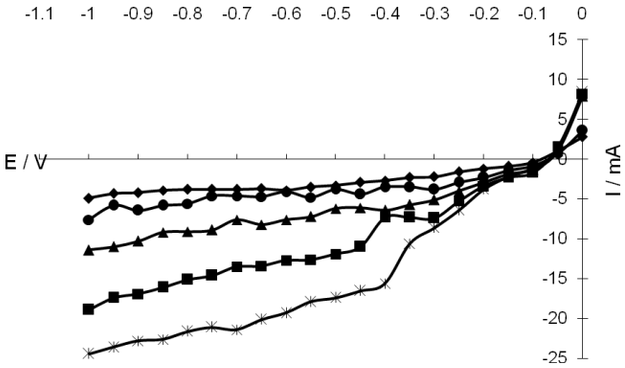

Fig. 6a. Observed limiting currents for Cu^{2+} cathodic reduction on P1 electrode (2 cm before the channel reactor) at different nominal *Re*: (◆) 194, (●) 387, (▲) 581, (■) 775, (∗) 969. Electrolyte, 10 mM $CuSO_4$, 0.05 M Na_2SO_4, pH2.

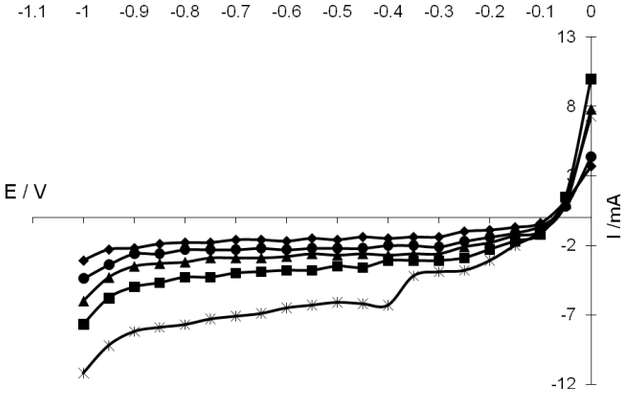

Fig. 6b. Observed limiting currents for Cu^{2+} cathodic reduction on P2 electrode (0.5 cm before the channel reactor) at different nominal *Re*: (◆) 194, (●) 387, (▲) 581, (■) 775, (∗) 969. Electrolyte, 10 mM $CuSO_4$, 0.05 M Na_2SO_4, pH2.

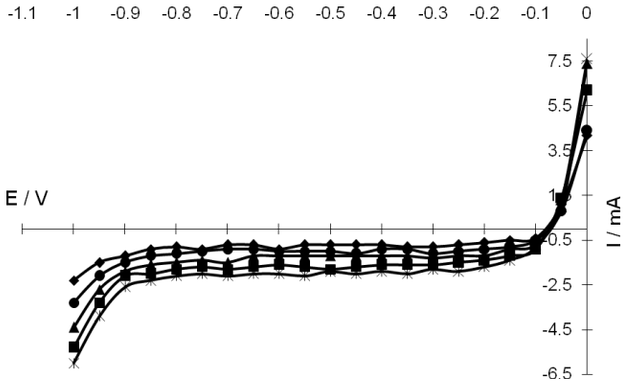

Fig. 6c. Observed limiting currents for Cu^{2+} cathodic reduction on P3 electrode (1 cm in the channel reactor) at different nominal *Re*: (◆) 194, (●) 387, (▲) 581, (■) 775, (∗) 969. Electrolyte, 10 mM $CuSO_4$, 0.05 M Na_2SO_4, pH2.

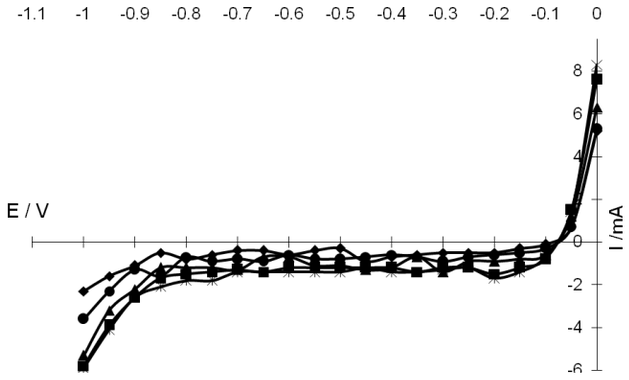

Fig. 6d. Observed limiting currents for Cu^{2+} cathodic reduction on P8 electrode (at the end of the channel length) at different nominal *Re*: (◆) 194, (●) 387, (▲) 581, (■) 775, (∗) 969. Electrolyte, 10 mM $CuSO_4$, 0.05 M Na_2SO_4, pH2.

Fig. 6c shows that for all nominal *Re* examined the limiting currents for Cu^{2+} cathodic reduction on electrode P3 (1.0 cm in the channel entry) are well defined. This suggests that the experimental mass transport is carried out in a fully developed laminar flow. According to CFD analysis (Fig. 3c) on P3 the fluid flow is developed for $194 < Re < 387$.

Experimental limiting currents for Cu^{2+} cathodic reductionin the whole channel length (10 cm), including the electrodes P3–P8, always present well defined plateaus. Fig. 6d shows the limiting currents on electrode P8. For this electrode, experimental limiting currents are not affected by the reactor outlet port. In general, experimental limiting currents for Cu^{2+} cathodic reduction do not need fully developed laminar flows. Very well defined plateaus can be found, applying Eqns. 1–3, in electrochemical reactors when simulated flow pattern presents a minimum flow maldistribution.

6. Conclusions

CFD offers the possibility for reducing the design costs for similar electrochemical reactors. Under this approach, it is possible to evaluate: a) the maximum cathode area at which the flow pattern describes a fully developed laminar flow; b) the flow pattern and its effect on mass transport in developing fluids along a reactor.

Good experimental limiting currents, for Cu^{2+} cathodic reduction, can be obtained when the simulated flow pattern presents a minimum flow maldistribution.

This approach could be attractive to reactor designers since it requires few physical parameters and facilitates preliminary characterization of geometrical configurations.

For the reactor studied here, the flow pattern assessment indicates that the Cu^{2+} cathodic reduction is possible at 10 mM under a broad nominal *Re* regime. Numerical results are in agreement with experimental ones.

Acknowledgment

The authors gratefully acknowledge the financial support of CONACyT program.

References

[1] J. Cui, L. Zhang. Metallurgical recovery of metals from electronic waste: a review, J. Hazard. Mater. 158 (2008) 228–256.
[2] F.C. Walsh. Electrochemical technology for environmental-treatment and clean energy conversion. Pure Appl. Chem. 73(12) (2001) 1819–1837.
[3] L.J.J. Janssen, L. Koene. The role of electrochemistry and electrochemical technology in environmental protection. Chem. Eng. Jl. 85 (2002) 137–146.
[4] D. Pletcher, F.C. Walsh. Industrial Electrochemistry, 2nd ed., Chapman & Hall. London, New York. 1993
[5] J. Blaedel, J.H. Strohl. Continuous quantitative electrolysis. Anal. Chem. 36 (1964) 1245–1251.
[6] A. Tentorio, U. Casolo-Ginelli. Characterization of reticulate, three-dimensional electrodes. J. Appl. Electrochem. 8 (1978) 195–205.
[7] J. Wang, H.D. Dewald. Deposition of metals at a flow-through reticulated vitreous carbon electrode coupled with on-line monitoring of the effluent. J. Electrochem. Soc. 130(9) (1983) 1814–1816.
[8] Q. Chu, J. Lianga, J. Hao. Electrodeposition of zinc-cobalt alloys from choline chloride–ureaionic liquid. Electrochim. Acta. 115 (2014) 499–503.
[9] H. Yang, R.G. Reddy. Electrochemical deposition of zinc from zinc oxide in 2:1 urea/choline chloride ionic liquid. Electrochim. Acta. 147 (2014) 513–519.
[10] M. Lia, Z. Wang, R.G. Reddy. Cobalt electrodeposition using urea and choline chloride. Electrochim. Acta. 123 (2014) 325–331.
[11] S. Fogarasi, F. Imre-Lucaci, P. Ilea, Á. Imre-Lucaci. The environmental assessment of two new copper recovery processes from waste printed circuit boards. J. Cleaner Prod. 54 (2013) 264–269.
[12] C. Ponce deLeon and D. Pletcher. The removal of Pb(II) from aqueous solutions using a reticulated vitreous carbon cathode cell—the influence of the electrolyte medium. Electrochim. Acta. 41(4) (1996) 533–541.
[13] D. Pletcher, I. Whyte, F.C. Walsh, J.P. Millington. Reticulated vitreous carbon cathodes for metal ion removal from process stream. Part I: Mass transport studies. J. Appl. Electrochem. 21 (1991) 659.
[14] D. Pletcher, I. Whyte, F.C. Walsh, J.P. Millington. Reticulated vitreous carbon cathodes for metal ion removal from process stream. Part II: Removal of copper (II) from acid sulphate media. J. Appl. Electrochem. 21 (1991) 667.
[15] F.C. Walsh, ed., A first course in electrochemical engineering. The Electrochemical Consultancy. Romsey, UK. 1993.
[16] D.J. Pickett, C.J. Wilson. Mass transfer in a parallel plate electrochemical cell—the effect of change of flow cross-section at the cell inlet. Electrochim. Acta. 27 (1982) 591–594.
[17] O. Levenspiel, ed., Chemical Reaction Engineering, Wiley, New York, 1972.
[18] P. Trinidad, F.C. Walsh. Hydrodynamic behaviour of the FM0-LC reactor. Electrochim. Acta. 4 (1996) 493–502.
[19] J.W. Baughn, N.A. Hoffman, N.A. Takahashi, B.E. Launder. Local heat transfer downstream of an abrupt expansion in a circular channel with constant wall heat flux. J. Heat Transfer. 106 (1984) 789–796.
[20] A.K. Runchal. Mass transfer investigation in turbulent flow downstreams of sudden enlargement of a circular pipe for very high Schmidt numbers. Int. J. Heat Mass Trans. 14 (1971) 781–792.
[21] D.J. Tagg, M.A. Patrick, A.A. Wragg. Heat and mass transfer downstream of abrupt nozzle expansions in turbulent flow. Trans. I. Chem. E57 (1979) 176–181.
[22] A. Djati, M. Brahimi, J. Legrand, B. Saidani. Entrance effect on mass transfer in a parallel plate electrochemical reactor. J. Appl. Electrochem. 31 (2001) 833–837.
[23] A. Frías-Ferrer, L. González-García, V. Sáez, C. Ponce de León, F.C. Walsh. The effects of manifold flow on mass transport in electrochemical filter-press reactors. AIChE J. 54 (2008) 811–823.

[24] J.L.C. Santos, V. Geraldes, S. Velizarov, J.G. Crespo. Characterization of fluid dynamics and mass-transfer in an electrochemical oxidation cell by experimental and CFD studies. Chem. Ing. J. 157 (2010) 379–392.
[25] L. Vázquez, A. Alvarez-Gallegos, F.Z. Sierra, C. Ponce de León, F.C. Walsh. Simulation of velocity profiles in a laboratory electrolyser using computational fluid dynamics. Electrochim. Acta. 55 (2010) 3437–3445.
[26] L. Vázquez, A. Alvarez-Gallegos, F.Z. Sierra, C. Ponce de León, F.C. Walsh. Prediction of mass transport profiles in a laboratory filter-press electrolyser by computational fluid dynamics modeling. Electrochim. Acta. 55 (2010) 3446–3453.
[27] L. Vázquez, A. Alvarez-Gallegos, F.Z. Sierra, C. Ponce de León, F.C. Walsh. CFD evaluation of internal manifold effects on mass transport distribution in a laboratory filter-press flow cell. J. Appl. Electrochem. 43 (2013) 453–465.
[28] H.K. Versteeg, W. Malalasekera. An Introduction to Computational Fluid Dynamics. Pearson Prentice Hall. Essex. 2007